Title

Real-Space Pseudopotential Method for the Calculation of Third-Row Elements X-ray Photoelectron Spectroscopic Signatures.

Journal

Journal of Chemical Theory and Computation, 20(14)

Authors

Liu, Liping

Xu, Qiang

Dos Anjos Cunha, Leonardo

et al.

Publication Date

2024-07-23

DOI

10.1021/acs.jctc.4c00535

JCTC Journal of Chemical Theory and Computation

pubs.acs.org/JCTC Article

Real-Space Pseudopotential Method for the Calculation of Third-Row Elements X-ray Photoelectron Spectroscopic Signatures

Liping Liu, Qiang Xu, Leonardo dos Anjos Cunha, Hongliang Xin, Martin Head-Gordon, and Jin Qian*

Cite This: J. Chem. Theory Comput. 2024, 20, 6134−6143 Read Online

ACCESS | Metrics & More | Article Recommendations | Supporting Information

ABSTRACT: X-ray photoelectron spectroscopy (XPS) is a powerful characterization technique that unveils subtle chemical environment differences via core−electron binding energy (CEBE) analysis. We extend the development of real-space pseudopotential methods to calculating 1s, 2s, and $2p_{3/2}$ CEBEs of third-row elements (S, P, and Si) within the framework of Kohn−Sham density-functional theory (KS-DFT). The new approach systematically prevents variational collapse and simplifies core-excited orbital selection within dense energy level distributions. However, careful error cancellation analysis is required to achieve accuracy comparable to all-electron methods and experiments. Combined with real-space KS-DFT implementation, this development enables large-scale simulations with both Dirichlet boundary conditions and periodic boundary conditions.

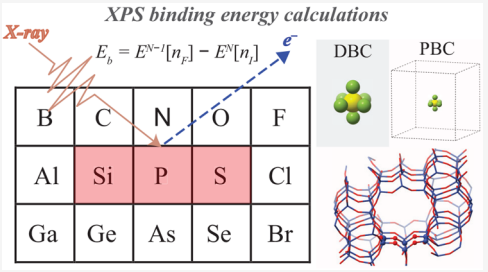

1. INTRODUCTION

X-ray photoelectron spectroscopy (XPS) is a widely used characterization technique that provides core−electron binding energies (CEBEs) in both molecules[1] and condensed matter.[2−4] In addition to element specificity, the same element in different local chemical environments can possess distinct CEBEs, differences of which can be referred to as binding energy shifts or chemical shifts[1] and can provide guidance in probing the local configurations of the elements.[5,6] This technique is traditionally applied in an ultrahigh vacuum setting. In recent years, ambient pressure XPS (apXPS) has been developed to accommodate in situ and operando experiments.[7,8] These exciting developments allow for simultaneously probing the electric field, the atomic concentration, and the interfacial structure.[9] In addition, time-resolved XPS (trXPS) is emerging as an effective probe for understanding ultrafast charge dynamics by tracking electronically and chemically sensitive, time-dependent CEBE shifts.[10] As more nuanced experiments lack well-established benchmarks and often require *ab initio* guidance, the need for theoretical prediction is surging.[11,12]

A variety of theoretical approaches are available for the estimation of CEBEs. The simplest approach is Koopman's theorem[5,13,14] using the negative of eigenvalues of the ground states as CEBEs. Slater's transition-state theory[15,16] or generalized Slater's transition-state theory[17,18] can estimate CEBEs by employing modified self-consistent field calculations for states with partially occupied core orbitals. A well-established approach is the Δ self-consistent field (ΔSCF) method[19−28] where the CEBEs are determined by the total energy differences between ground and core-excited states. Post-HF methods represents another popular class of approaches for estimating CEBEs, which includes but not limited to, configuration interaction,[29,30] coupled cluster singles and doubles (CCSD)[31−37] or equation of motion coupled cluster (EOM-CCSD).[38−40] Lastly, the quasiparticle GW methods[41−45] based on the Green's function can provide an accurate and dynamic response of a system to a core-hole but suffer from high computational cost.

Here we focus on one of the most widely used KS-DFT based ΔSCF approach as it strikes a good balance between the accuracy and efficacy in CEBEs calculations. The ΔSCF approach within an all-electron (AE) framework has been extensively benchmarked and studied for both molecules[23,25,46] and condensed matter.[28,47,48] Recent studies[17,47] showed that the SCAN exchange-correlation functional[49] can achieve high numerical accuracy, with a mean absolute error (MAE) of ∼0.2 eV, for calculating absolute CEBEs (E_b) of elements in both molecules and solids. However, AE calculations suffer from variational collapse toward the lower energy states or ground states[50] unless appropriate SCF solvers are not used, such as maximum overlap method (MOM),[51] σ self-consistent field method (σ-SCF),[52,53] and so on. Furthermore, AE calculations are computationally intractable for large-scale systems, thereby hindering its practical application. Parallel to the AE approaches, ΔSCF calculations based on pseudopotentials (PP)[24,54−63] have also been performed, showing general agreement with experimental measurements in terms of

Received: April 21, 2024
Revised: June 18, 2024
Accepted: June 20, 2024
Published: July 6, 2024

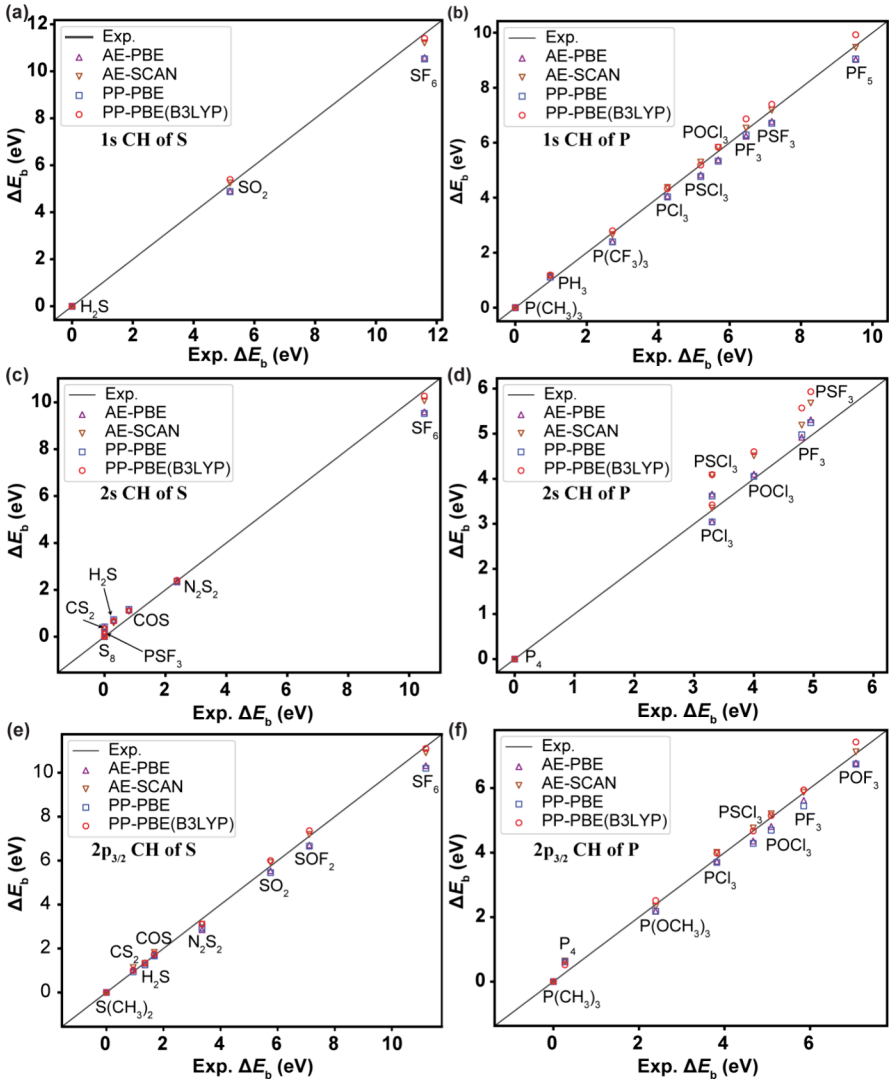

Figure 1. Binding energy shifts of 1s (a, b), 2s (c, d), and $2p_{3/2}$ (e, f) core excitations of molecules for S and P elements, respectively. More details can be found in Tables S1, S2, S3, and S4 in the Supporting Information.

CEBE shifts ($\Delta E_b = E_b - E_{ref}$, E_{ref} is an arbitrary reference system).

In a previous study,[50] we proposed a PP approach within the ΔSCF scheme of real-space KS-DFT for the calculations of 1s CEBEs of second-row elements. Using Dirichlet boundary condition (DBC), the PP approach showed comparable MAE of ΔE_b with those obtained from the AE approach. However, the applicability of this method for heavier elements, as well as its implications under periodic boundary conditions (PBC) are still unclear. Herein, we extend this PP strategy to the calculations of 1s, 2s, and $2p_{3/2}$ CEBEs of third-row elements (S and P), benchmarked with state-of-art AE approaches[64−66] and experiments. Compared to AE calculations, this PP approach exhibits excellent numerical stability and simplifies selections for core-excited orbitals, especially for condensed orbital spaces where multiple orbitals display similar energy levels, thereby significantly lowering the adoption barrier for users. Furthermore, it shows comparable accuracy to the state-of-art AE calculations in terms of ΔE_b. Lastly, we devise strategies to extend this PP approach to PBC by carefully discussing and leveraging error cancellation. By either correcting Coulomb interactions between periodic replicas or employing large, fixed supercells, we can arrive at a satisfactory ΔE_b for periodic systems. Hence, embedded in real-space KS-DFT, this method enables the calculations of CEBEs of large-scale systems using both DBC or PBC, which will be useful for applications in areas such as surface science, catalysis, and energy storage.

2. RESULTS AND DISCUSSION

2.1. Computational Details. *Pseudopotential Approach.* Within the ΔSCF scheme,[23] the E_b can be obtained by eq 1,

$$E_b = E^{N-1}[n_F] - E^N[n_I] \tag{1}$$

where $E^N[n_I]$ and $E^{N-1}[n_F]$ are the total energies of the initial states (ground states) and corresponding final states (the core-excited states with core-holes), respectively, and N is the total number of electrons of the initial state.

Our recent work[50] derived the AE total energies for the final and initial states using the definition of cohesive energy:

$$E[n] \simeq E[\rho] - \sum_a^{N_a} E[\rho_a] + \sum_a^{N_a} E[n_a] \tag{2}$$

https://doi.org/10.1021/acs.jctc.4c00535
J. Chem. Theory Comput. 2024, 20, 6134−6143

Table 1. Mean Absolute Errors of 1s, 2s, and $2p_{3/2}$ Binding Energy Shifts of S and P in Molecules with Respect to the Experiments[a]

CH	Element	AE-PBE	AE-SCAN	PP-PBE	PP-PBE (B3LYP)
1s	S	0.65	0.22	0.70	0.20
	P	0.30	0.09	0.32	0.19
2s	S	0.38	0.26	0.40	0.23
	P	0.24	0.49	0.22	0.65
$2p_{3/2}$	S	0.32	0.16	0.33	0.14
	P	0.25	0.13	0.31	0.15

[a]The numbers in this table are indicated in eV.

where N_a is the number of atoms in the simulation systems, n and ρ denote the AE and PP electron densities, respectively, and $E[n_a]$ and $E[\rho_a]$ are the AE and PP energies of the a-th isolated atom, respectively, which can be conveniently obtained during the PP generation. Combining eqs 1 and 2, the E_b are obtained from PP calculations for final and initial states. A detailed derivation can be found in our previous work.[50] The success of this approach is attributed to the fact that the PP calculations can provide a good approximation of cohesive energies as those obtained from AE calculations. The PPs derived from the AE calculations of isolated atoms can accurately replicate the AE potentials outside of pseudocore regions.[67] Given the inertness of core electrons in chemical reactions, this alignment facilitates the accurate evaluation of the interaction energies between valence electrons and pseudocores, ensuring the transferability of these PPs across different chemical environments. Note that if core−valence mixing becomes considerable, a harder PPs should be employed, where more core electrons are excluded from the frozen pseudocores during the PP generation.

All calculations via the PP approach are performed in the real-space ARES package.[68] As structures from the B3LYP functional only marginally improve the accuracy of the E_b predictions (Table S1), geometry optimization is performed in Q-Chem[69] with the PBE functional[70] and the cc-pVTZ basis set.[71] Troullier-Martins (TM) PPs[72] with 1s, 2s, and 2p core-holes are generated using the FHI98PP code[73] to represent the atoms with core-holes, respectively. General TM PPs are used to describe the atoms that are not core-excited. This assignment intrinsically localizes a core-hole to a specific core-excited atom, which is analogous to the mixed basis strategy used in the AE calculations.[65] Especially for species with equivalent atoms, this approach effectively breaks the equivalence, thereby avoiding hole delocalization among equivalent atoms. With the fully screened core-hole assumption,[5] these PPs can be implemented into the ARES package for calculations of initial and final states via the traditional SCF

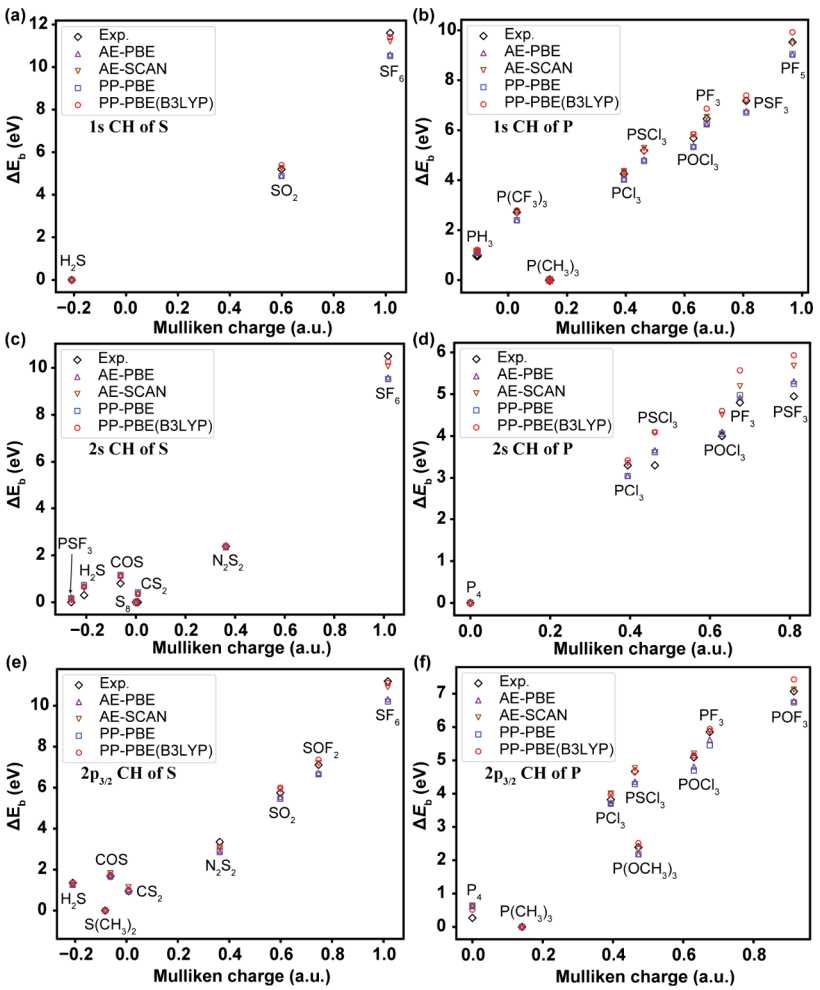

Figure 2. Binding energy shifts of 1s (a, b), 2s (c, d), and $2p_{3/2}$ (e, f) core excitations versus the Mulliken charges of molecules for S and P elements, respectively.

https://doi.org/10.1021/acs.jctc.4c00535
J. Chem. Theory Comput. 2024, 20, 6134−6143

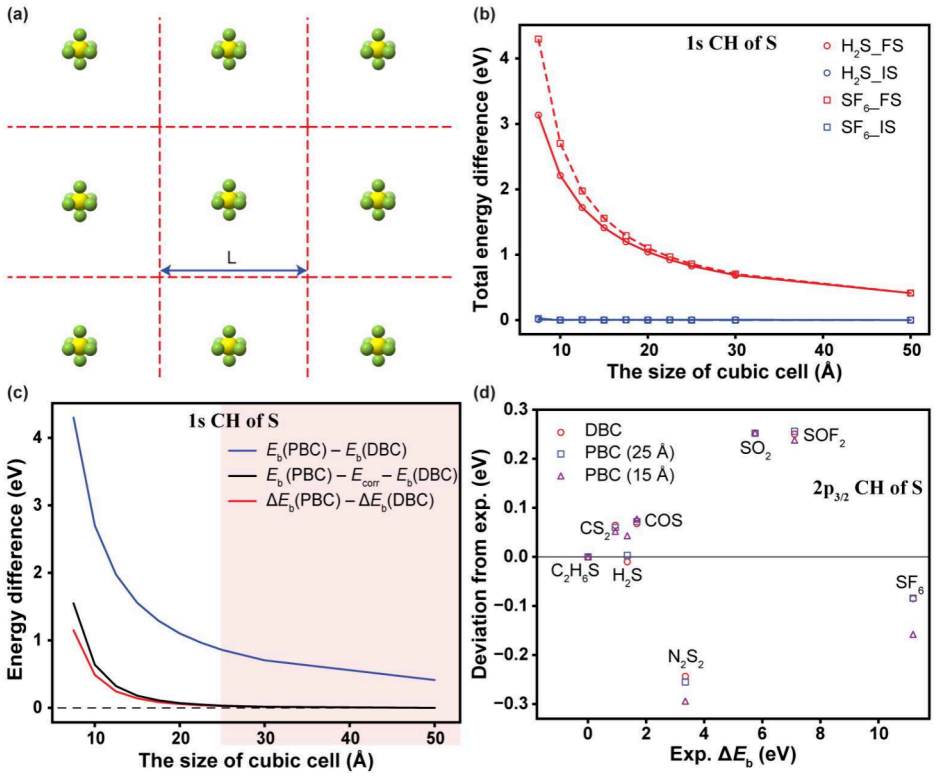

Figure 3. Numerical results within PBC. (a) Illustration of charged molecules within the PBC. (b) Total energy convergence with respect to the cell sizes of initial and final states with 1s core-holes for H_2S and SF_6 molecules. The total energy differences are computed by the energy differences between the final/initial states within PBC and the corresponding states within DBC. (c) the convergence of 1s CEBEs of SF_6 with respect to the cell size. (d) $2p_{3/2}$ ΔE_b of S-containing molecules within PBC with the cell sizes of 15 and 25 Å, respectively, in comparison to experiments and that within DBC. E_b and ΔE_b are available in Table S5. MAE of PBC (15 Å) and PBC (25 Å) are 0.15 and 0.14 eV, respectively, which shows excellent consistency with that of DBC. The results are generated using the PP−PBE(B3LYP) method.

iterations. Note that the PPs with 2p core-holes are spherically symmetric and can thus be interpreted as the average of those with $2p_{1/2}$ and $2p_{3/2}$ core holes. Consequently, $2p_{3/2}$ CEBEs can be effectively extrapolated from the calculations with the TM PPs. This method resembles the multiplet average scheme[66] used in the AE approaches. To improve the accuracy of the calculations of ΔE_b at a low computational cost, the one-shot B3LYP-refining step proposed in ref[50] is adopted by using the PBE-optimized KS orbitals and electron density as input, and B3LYP energy as output. The PP methods using PBE functional and B3LYP-refining step are denoted as PP−PBE and PP−PBE(B3LYP), respectively, adopting a consistent nomenclature with our previous work.[50,74]

All-Electron Approach. AE calculations, together with experimental data,[1] serve as valuable benchmarks for the developed PP approach. Within the AE framework, the total energy can be obtained by explicitly relaxing all the core and valence electrons. As the core-holes represent non-Aufbau solutions to the SCF equations, specialized solvers need to be used to avoid variational collapses and refilling of the core-holes in AE calculations.

AE calculations for CEBEs of third-row elements are performed with the Q-Chem package.[69] Molecular structures are optimized with the PBE functional[70] and the cc-pVTZ basis set[71] as the B3LYP functional[75] only slightly improves the accuracy of AE calculations (Table S2), consistent with those in the PP calculations. It is worth pointing out that the AE methods adopted in our previous report for second-row elements[50] are not sufficiently accurate for the third-row elements and shows a high MAE (~0.3 eV) for calculating ΔE_b (Table S2). The low accuracy of these AE methods is largely due to incompleteness of the cc-pVTZ basis set and the omission of nontrivial relativistic effects, which are important for heavier elements. Moreover, the selection of basis set has been shown to impact both the accuracy and efficiency of AE calculations.[44] Thus, in this manuscript, the aug-pcX-2 basis set[76] is used, and scalar relativistic effects are incorporated through the exact two-component (X2C) Hamiltonian.[66] The semilocal meta-GGA SCAN functional[49] together with the PBE[70] and B3LYP[75] functionals are employed for benchmarking. Local exchange-correlation integrals for all density functional approximations are calculated over a radial grid with 99 points and an angular Lebedev grid with 590 points on each radial sphere. ΔSCF calculations with the maximum overlap method[51] (MOM) are carried out to obtain core-ionized states. For more complex cases, such as S_8 and P_4, the square gradient minimization (SGM)[65,77] protocol is employed to prevent variational collapse. For species with more than a single equivalent atom (e.g., S in CS_2), the Boys localization[78] procedure is used to localize the core-hole onto a single site. Finally, spin−orbit coupling effects are accounted for through the multiplet average scheme introduced in ref[66] to obtain the $2p_{3/2}$ CEBEs. The convergence threshold for all core-ion calculations is set to 10^{-5} a.u.

The ΔE_b for 1s core-hole of S and P elements performed by AE calculations with different input parameters are summarized in Table S2. Interestingly, the SCAN functional with the aug-pcX-2 basis set and inclusion of scalar relativistic effects

https://doi.org/10.1021/acs.jctc.4c00535
J. Chem. Theory Comput. 2024, 20, 6134−6143

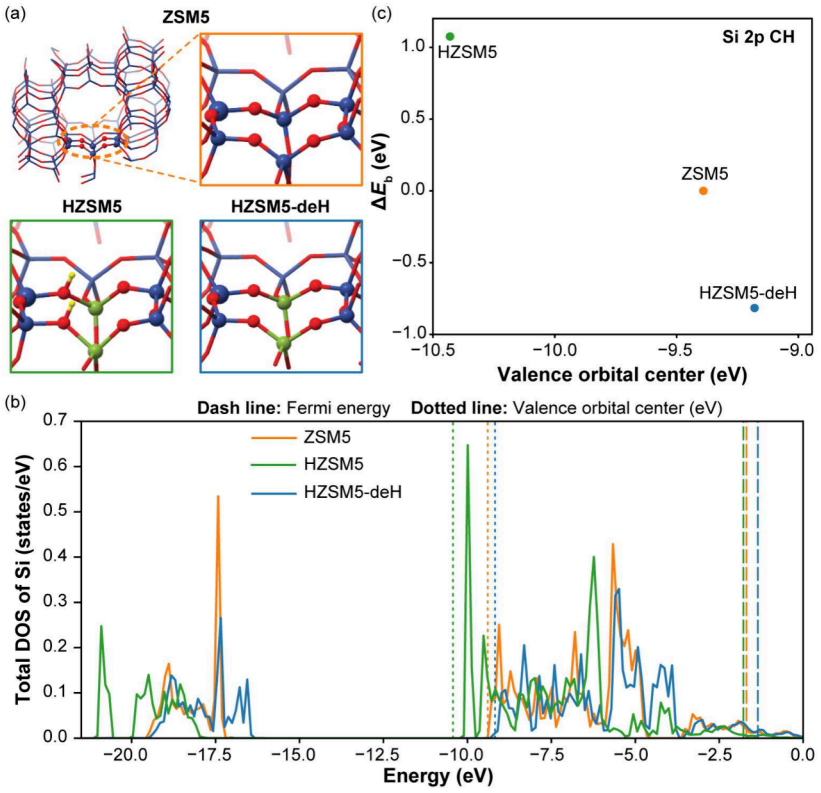

Figure 4. Si-2p CEBEs in the ZSM-5 zeolite series. (a) Structures of the ZSM5, HZSM5, and HZSM5-deH. (b) Total DOS of the Si cations. (c) Si-2p ΔE_b with respect to the valence orbital centers. The Si cations with core-holes are highlighted with enlarged representation. Color code: Si, blue; O, red; Al, green; H, yellow.

(denoted as AE-SCAN) is the best AE approach for the calculations of both E_b and ΔE_b of 1s core electrons of the third-row elements. AE methods using PBE and B3LYP functionals are labeled as AE-PBE and AE-B3LYP, respectively.

2.2. Numerical Results within DBC. The real-space KS-DFT code ARES[68] allows for calculations with either PBC or DBC. However, it is challenging to model the core-excited states of systems within PBC because of the long-range electrostatic interactions between the periodic replicas. Even if uniform compensation charges are included in the supercell, the nonconvergence of the periodically charged final states is demonstrated in this work (Figure 3b). Adopting one of the many mathematical schemes[28,43,79−81] that numerically correct or counteract the Coulomb interactions is usually imperative but daunting. Thus, we first benchmark our PP development within DBC for calculating ΔE_b of third-row elements in isolated molecules. Thereafter, we compare our results with the AE and experimental results. In the following section, we will discuss the implications for extending this approach to PBC.

Prior to the CEBE calculations for third-row elements, we tested our AE and PP methods on ethyl trifluoroacetate (Table S3), also known as the ESCA molecule, as its C 1s chemical shifts serve as a critical reference and benchmark for XPS calculation methods.[45] Compared to experiments,[82] our developed PP−PBE(B3LYP) method achieves a high accuracy with MAE of 0.14 eV, which is comparable to that (0.13 eV) of ΔPBEh in ref.[45] This result reaffirms the efficacy of our PP approach for second-row elements.[50] To further validate the transferability and generalizability of this PP approach for heavier elements, a broad range of S- and P-containing molecules with distinct chemical environments were chosen in this study. Consistent with our previous report,[50] the E_b values obtained via the PP approach deviate considerably from experimental results, partly due to the neglect of spin polarization and relativistic effects when constructing the pseudopotentials (Table S1). Fortunately, these errors tend to cancel out when computing ΔE_b.[50] The 1s, 2s, and $2p_{3/2}$ ΔE_b of S- and P-containing molecules are calculated with respect to the molecules with the lowest E_b in each category: H_2S and $P(CH_3)_3$, S_8 and P_4, $S(CH_3)_2$ and $P(CH_3)_3$, respectively. All values of E_b and ΔE_b are summarized in Table S1−S5. The calculated ΔE_b of the corresponding core-holes from the PP approach in ARES, AE calculations in Q-Chem, and the experiments are illustrated in Figure 1. There is a systematic overlap between the results from the PP−PBE and those from AE-PBE, indicating that the PP approach can achieve the accuracy level of the AE approach, if the same functional is used. All PP results can reproduce the trends of ΔE_b in experiments (Figure 1).

It is worthwhile to point out that the PP approach with frozen core-holes intrinsically exhibits high numerical stability for all calculations. On the other hand, the AE calculations for core excited states, especially for molecules with multiple equivalent atoms, require careful use of specialized algorithms to avoid variational collapse as well as to localize the core-holes, as discussed in the Computational Details subsection. Furthermore, the PP approach simplifies the selection of the desired core excitation by assigning specific core-hole pseudopotentials to the targeted atom. By contrast, at present, the AE approach requires manual identification of the core excitation orbital, which is nontrivial when the orbital space is dense, such as the 2s excitation of P in $PSCl_3$.

https://doi.org/10.1021/acs.jctc.4c00535
J. Chem. Theory Comput. 2024, 20, 6134−6143

The MAEs of ΔE_b from the PP approach are summarized in Table 1, for quantitative comparison with the AE approach. The PP−PBE has comparable accuracy as AE-PBE. Consistent with our previous report, the AE-PBE(B3LYP), using a nonself-consistent B3LYP refining step, demonstrates systematically improved accuracy for ΔE_b of 1s, 2s, and $2p_{3/2}$ core-holes, as compared to the AE-PBE, proving its universality and robustness in calculating ΔE_b. The only exceptions appear to be the 2s excitations of P, but we observe that those systems also exhibit apparently poor results using the AE methods (compare AE-SCAN and AE-PBE in Figure 1d and Table 1 with experiments). This consistent exception may be attributed to the poor quality of the experimental data set for 2s core-hole of P. Compared to the AE-SCAN method, the AE-PBE-(B3LYP) shows slightly worse MAEs of ΔE_b. Evidently, the AE approach with appropriate XC functionals, state-of-art basis sets and explicit relativistic effect can accurately describe the physics of final core-excited states, and hence exhibit much better E_b and slightly better ΔE_b than the PP approach. In summary, on par with the AE approach, the PP approach with frozen core-holes is a robust methodology for calculating XPS binding energies with high numerical stability and ease of usage, especially for large-scale systems. However, this comes at the cost of relying on error cancellation and the sacrifice of part of physical and numerical accuracy.

To further rationalize the generalizability of the present methodology for estimating CEBEs of elements in a wide range of chemical environments, we can employ a simple charge model due to Siegbahn.[83] This model pointed out the positive correlation between atomic charges and XPS binding energies. The calculated ΔE_b versus Mulliken charges are illustrated in Figure 2. We show that the ΔE_b in a broad range generally exhibits a positive correlation with the atomic charges. This phenomenon arises because a positively charged atom experiences reduced electrostatic repulsion, allowing it to tightly hold its core electrons, ultimately resulting in larger values for its CEBEs.

2.3. Implication for Periodic Systems. XPS has also been extensively utilized in a range of condensed matter systems, including bulk solids, surfaces, and interfaces. As these systems are inherently periodic and usually lack well-established benchmarks, accurate prediction of CEBEs of these systems is pivotal for interpreting XPS data and discerning the local chemical environments of atoms. This holds significant applications in diverse scientific topics, such as surface science,[84] catalysis,[85] and energy storage.[86] In the final core-hole states within PBC, the localization of the core-holes within PPs' pseudocores breaks the translational symmetry in the systems,[87] thus resulting in the nonconvergence of their total energies (Figure 3a, b). By treating these localized core-holes as point charges, the electrostatic interactions among periodic core-holes (E_{corr})[28] can be accurately assessed by using the Makov-Payne equation:[79]

$$E_{corr} = \frac{q^2\alpha}{2\epsilon L} \tag{3}$$

where q is the charge of the core-hole and equal to 1 e, α is the Madelung constant, ϵ is the dielectric constant of the material, and L is the cell size. The Madelung constant is dependent on the shape of the supercell. It is imperative to acknowledge that the Makov-Payne equation is not applicable for periodic systems where their electron holes are delocalized.[87]

Based on eq 3, two strategies can be introduced to ensure the accurate prediction of CEBEs of atoms within large-scale systems using PBC, including: 1) applying the E_{corr} to the final core-hole states, 2) calculating the ΔE_b within an identical supercell by canceling out the Coulomb interactions. To examine the performance of these strategies, we apply PBC with different cell sizes to the calculations of 1s CEBEs of S-containing molecules. The value of $\frac{\alpha}{\epsilon}$ of eq 3 in our system is determined by the E_{corr} at the cell size of 50 Å, where E_{corr} is equal to E_b (PBC)−E_b (DBC) . Notably, while the E_b of SF_6 under PBC fails to coverage, both $E_b - E_{corr}$ and the ΔE_b demonstrate convergence at the cell size of 25 Å (Figure 3c). This result suggests that for a large supercell, in this case >25 Å, the final state core-hole can be sufficiently represented by point charges, and therefore, the interaction errors can be safely canceled out when one employs a sufficiently large supercell.

From a practical point of view, we now analyze and compare the convenience of usage for these two strategies. We note that significant attention is needed for strategy 1). The calculation of E_{corr} is nontrivial because of the difficulty associated with obtaining both the dielectric constant and the Madelung constant. To obtain the $\frac{\alpha}{\epsilon}$ of eq 3, linear fitting E_b with $\frac{1}{L}$ is required.[28] In contrast, the strategy 2) ensures the accurate prediction of ΔE_b by employing a large, identical supercell and thus canceling out the E_{corr}. To further validate the applicability and generalizability of the strategy 2), the $2p_{3/2}$ ΔE_b of S element across various chemical environments are calculated by ARES within PBC with different cell sizes (Figure 3d). As expected, when setting the supercell size to 25 Å, the $2p_{3/2}$ ΔE_b of S within PBC is consistent with the results obtained within DBC. Interestingly, we also observe that a large part of the Coulomb interaction error cancels out for systems with an even smaller supercell, such as 15 Å. In this context, the large difference of numerical values obtained in DBC (or PBC at 25 Å) and PBC at 15 Å, for example in H_2S, SF_6, and N_2S_2, results from large bond dipoles that interact strongly with nearby core-holes.

2.4. Demonstration of a Large System. Lastly, to illustrate the advantage of the present real-space KS-DFT PP development in simulating large-scale, periodic systems, we turn to ZSM-5 zeolite series which are widely used as catalysts or supports of catalysts for various industrial processes.[88−90] The Al/Si ratios and the densities of Brønsted acid sites (the protons on the O linking to the framework Al^{3+}) are key features of ZSM-5 zeolites, determining their efficacy in catalysis and their capabilities in anchoring catalysts. However, it is often challenging to quantify these features in experiments. XPS can serve as a powerful tool for discerning the chemical environments of Si cations adjacent to the framework Al^{3+} or Brønsted acid sites, facilitating the identification of these important sites.

To ensure the applicability of the aforementioned strategy 2), we adopt a $p(1 \times 1 \times 2)$ supercell with ∼580 atoms and a large cell size of 20.383 × 19.534 × 26.994 Å. Computational details for the structure optimizations of the ZSM-5 zeolite series can be found in ref.[88] We then calculate the Si-2p ΔE_b in Al-substituted ZSM-5 with Bronsted acid sites (HZSM5) and deprotonated counterparts (HZSM5-deH) with respect to the pristine ZSM-5 (ZSM5) (Figure 4). The results show that Si-2p E_b of HZSM5 is elevated relative to ZSM5, while HZSM5-deH exhibits the lowest value. To elucidate the observed shifts

https://doi.org/10.1021/acs.jctc.4c00535
J. Chem. Theory Comput. 2024, 20, 6134−6143

in the Si-2p E_b, we employ the orbital centers of Si valence electrons[91] as a descriptor, which can be computed from the total DOS of the Si cations (Figure 4b). The position of valence orbital center is a representation of the averaged energy level of Si valence electrons. The Si centers with the lower valence electron levels is expected to also have lower core electron levels, thereby resulting in larger (more positive) 2p CEBE. In accordance with the Koopman's theorem,[5] we rationalize that the valence orbital centers are inversely correlated with 2p CEBEs, as shown in Figure 4c. Our calculations suggest that theoretical XPS predictions have the exciting potential for differentiating important catalytic active centers, at a resolution that was traditionally unachievable via experiments alone.

3. CONCLUSION

In sum, a real-space PP method for the calculation of 1s, 2s, and $2p_{3/2}$ CEBEs of the third-row elements has been developed. The performance of this PP development within DBC and PBC are benchmarked with high quality AE methods as well as experiments. Roughly 0.2 eV accuracy (MAE) has been achieved with the one-shot B3LYP strategy and careful error-cancellation analysis has been presented. The developed PP approach exhibits superior numerical stability and simplifies selections for core-excited orbitals. Combined with the efficient real-space KS-DFT implementations, this method provides advantages for calculating accurate core−electron binding energies of large-scale systems.

■ ASSOCIATED CONTENT

Supporting Information

The Supporting Information is available free of charge at https://pubs.acs.org/doi/10.1021/acs.jctc.4c00535.

Summary of calculated Mulliken charges and all CEBE data (PDF)

Optimized structures, PPs for ground states and core-excited states, AE calculation inputs, and PPs calculation inputs (ZIP)

■ AUTHOR INFORMATION

Corresponding Author

Jin Qian − *Chemical Sciences Division, Lawrence Berkeley National Laboratory, Berkeley, California 94720, United States;* orcid.org/0000-0002-0162-0477; Email: jqian2@lbl.gov

Authors

Liping Liu − *Department of Chemical Engineering, Virginia Polytechnic Institute and State University, Blacksburg, Virginia 24060, United States;* orcid.org/0000-0001-7543-1751

Qiang Xu − *Chemical Sciences Division, Lawrence Berkeley National Laboratory, Berkeley, California 94720, United States;* orcid.org/0000-0003-3747-4325

Leonardo dos Anjos Cunha − *Department of Chemistry, University of California, Berkeley, Berkeley, California 94720, United States; Chemical Sciences Division, Lawrence Berkeley National Laboratory, Berkeley, California 94720, United States;* orcid.org/0000-0003-2671-2375

Hongliang Xin − *Department of Chemical Engineering, Virginia Polytechnic Institute and State University, Blacksburg, Virginia 24060, United States;* orcid.org/0000-0001-9344-1697

Martin Head-Gordon − *Department of Chemistry, University of California, Berkeley, Berkeley, California 94720, United States; Chemical Sciences Division, Lawrence Berkeley National Laboratory, Berkeley, California 94720, United States;* orcid.org/0000-0002-4309-6669

Complete contact information is available at: https://pubs.acs.org/10.1021/acs.jctc.4c00535

Notes

The authors declare no competing financial interest.

■ ACKNOWLEDGMENTS

This work was primarily supported by the U.S. Department of Energy (DOE), Office of Science, Basic Energy Sciences, Chemical Sciences, Geosciences, and Biosciences Division, under Contract No. DE-AC02-05CH11231. J.Q was supported by the DOE Early Career Research Program, and M.H.G. and L.A.C. were supported by the Atomic Molecular and Optical Sciences Program for development of the X2C capability. M.H.G. and L.A.C. received additional support from DOE BES under Award DE-SC0021266 (Liquid Sunlight Alliance), for the assessment of different density functionals. L.L. and H.X. acknowledge support from the NSF Chemical Catalysis program (CHE-2102363). L.L. thanks the NSF Non-Academic Research Internships for Graduate Students (INTERN) program for supporting his work in the Lawrence Berkeley National Laboratory under the guidance of J.Q.

■ REFERENCES

(1) Jolly, W. L.; Bomben, K. D.; Eyermann, C. J. Core-electron binding energies for gaseous atoms and molecules. *At. Data Nucl. Data Tables* **1984**, *31*, 433−493.

(2) Siegbahn, K. Electron spectroscopy for atoms, molecules, and condensed matter. *Rev. Mod. Phys.* **1982**, *54*, 709−728.

(3) Niedermaier, I.; Kolbeck, C.; Taccardi, N.; Schulz, P. S.; Li, J.; Drewello, T.; Wasserscheid, P.; Steinrück, H.-P.; Maier, F. Organic reactions in ionic liquids studied by in situ XPS. *ChemPhysChem* **2012**, *13*, 1725−1735.

(4) Lam, R. K.; Smith, J. W.; Rizzuto, A. M.; Karslıoğlu, O.; Bluhm, H.; Saykally, R. J. Reversed interfacial fractionation of carbonate and bicarbonate evidenced by X-ray photoemission spectroscopy. *J. Chem. Phys.* **2017**, *146*, 094703.

(5) Egelhoff, W. F. Core-level binding-energy shifts at surfaces and in solids. *Surf. Sci. Rep.* **1987**, *6*, 253−415.

(6) Pueyo Bellafont, N.; Viñes, F.; Illas, F. Performance of the TPSS Functional on Predicting Core Level Binding Energies of Main Group Elements Containing Molecules: A Good Choice for Molecules Adsorbed on Metal Surfaces. *J. Chem. Theory Comput.* **2016**, *12*, 324−331.

(7) Ali-Löytty, H.; Louie, M. W.; Singh, M. R.; Li, L.; Sanchez Casalongue, H. G.; Ogasawara, H.; Crumlin, E. J.; Liu, Z.; Bell, A. T.; Nilsson, A.; Friebel, D. Ambient-Pressure XPS Study of a Ni-Fe Electrocatalyst for the Oxygen Evolution Reaction. *J. Phys. Chem. C* **2016**, *120*, 2247−2253.

(8) Zhang, X.; Govindarajan, N.; He, X. et al. Hydrogen bond network at the H2O/solid interface. *Encyclopedia of Solid-Liquid Interface*. 2024, p 92

(9) Head, A. R. *Ambient Pressure Spectroscopy in Complex Chemical Environments*; American Chemical Society 2021; Vol. *1396*; pp 19−37.

(10) Neppl, S.; Gessner, O. Time-resolved X-ray photoelectron spectroscopy techniques for the study of interfacial charge dynamics. *J. Electron Spectrosc. Relat. Phenom.* **2015**, *200*, 64−77.

(11) Hao, H.; Ruiz Pestana, L.; Qian, J.; Liu, M.; Xu, Q.; Head-Gordon, T. Chemical transformations and transport phenomena at interfaces. *Wiley Interdiscip. Rev. Comput. Mol. Sci.* **2023**, *13*, e1639.
(12) Besley, N. A. Modeling of the spectroscopy of core electrons with density functional theory. *Wiley Interdiscip. Rev. Comput. Mol. Sci.* **2021**, *11*, e1527.
(13) Kowalczyk, S. P.; Ley, L.; Martin, R. L.; McFeely, F. R.; Shirley, D. A. Relaxation and final-state structure in XPS of atoms, molecules, and metals. *Faraday Discuss. Chem. Soc.* **1975**, *60*, 7−17.
(14) Carravetta, V.; Iucci, G.; Ferri, A.; Russo, M. V.; Stranges, S.; de Simone, M.; Polzonetti, G. Synchrotron radiation photoemission study of some π-conjugated alkynes in the gas phase: Experiment and theory. *Chem. Phys.* **2001**, *264*, 175−186.
(15) Triguero, L.; Plashkevych, O.; Pettersson, L. G. M.; Ågren, H. Separate state vs. transition state Kohn-Sham calculations of X-ray photoelectron binding energies and chemical shifts. *J. Electron Spectrosc. Relat. Phenom.* **1999**, *104*, 195−207.
(16) Hirao, K.; Nakajima, T.; Chan, B.; Lee, H.-J. The core ionization energies calculated by delta SCF and Slater's transition state theory. *J. Chem. Phys.* **2023**, *158*, 064112.
(17) Jana, S.; Herbert, J. M. Slater transition methods for core-level electron binding energies. *J. Chem. Phys.* **2023**, *158*, 094111.
(18) Hirao, K.; Nakajima, T.; Chan, B. An improved Slater's transition state approximation. *J. Chem. Phys.* **2021**, *155*, 034101.
(19) Bagus, P. S. Self-Consistent-Field Wave Functions for Hole States of Some Ne-Like and Ar-Like Ions. *Phys. Rev.* **1965**, *139*, A619−A634.
(20) Broughton, J. Q.; Perry, D. L. Calculation of adsorbate relaxation energies in X-ray photoelectron spectroscopy. *J. Chem. Soc., Faraday Trans. 2* **1977**, *73*, 1320−1327.
(21) Bagus, P. S.; Seel, M. Molecular-orbital cluster-model study of the core-level spectrum of CO adsorbed on copper. *Phys. Rev. B Condens. Matter* **1981**, *23*, 2065−2075.
(22) Bagus, P. S.; Rossi, A. R.; Avouris, P. CO core-excited states for CO/Cu(100): A cluster-model study. *Phys. Rev. B Condens. Matter* **1985**, *31*, 1722−1728.
(23) Qian, J.; Crumlin, E. J.; Prendergast, D. Efficient basis sets for core-excited states motivated by Slater's rules. *Phys. Chem. Chem. Phys.* **2022**, *24*, 2243−2250.
(24) Flynn, C. P.; Lipari, N. O. Soft-X-Ray Absorption Threshold in Metals, Semiconductors, and Alloys. *Phys. Rev. B Condens. Matter* **1973**, *7*, 2215−2229.
(25) Segala, M.; Takahata, Y.; Chong, D. P. Density functional theory calculation of 2p core-electron binding energies of Si, P, S, Cl, and Ar in gas-phase molecules. *J. Electron Spectrosc. Relat. Phenom.* **2006**, *151*, 9−13.
(26) Chong, D. P. Density-functional calculation of core-electron binding energies of C, N, O, and F. *J. Chem. Phys.* **1995**, *103*, 1842−1845.
(27) Chong, D. P.; Gritsenko, O. V.; Baerends, E. J. Interpretation of the Kohn-Sham orbital energies as approximate vertical ionization potentials. *J. Chem. Phys.* **2002**, *116*, 1760−1772.
(28) Kahk, J. M.; Michelitsch, G. S.; Maurer, R. J.; Reuter, K.; Lischner, J. Core Electron Binding Energies in Solids from Periodic All-Electron Δ-Self-Consistent-Field Calculations. *J. Phys. Chem. Lett.* **2021**, *12*, 9353−9359.
(29) Nelson, A. J.; Reynolds, J. G.; Roos, J. W. Core-level satellites and outer core-level multiplet splitting in Mn model compounds. *J. Vac. Sci. Technol. A* **2000**, *18*, 1072−1076.
(30) Hanson-Heine, M. W. D.; George, M. W.; Besley, N. A. A scaled CIS(D) based method for the calculation of valence and core electron ionization energies. *J. Chem. Phys.* **2019**, *151*, 034104.
(31) Purvis, G. D., III; Bartlett, R. J. A full coupled-cluster singles and doubles model: The inclusion of disconnected triples. *J. Chem. Phys.* **1982**, *76*, 1910−1918.
(32) Bartlett, R. J.; Musiał, M. Coupled-cluster theory in quantum chemistry. *Rev. Mod. Phys.* **2007**, *79*, 291−352.
(33) Zheng, X.; Cheng, L. Performance of delta-coupled-cluster methods for calculations of core-ionization energies of first-row elements. *J. Chem. Theory Comput.* **2019**, *15*, 4945−4955.
(34) Zheng, X.; Zhang, C.; Jin, Z.; Southworth, S. H.; Cheng, L. Benchmark relativistic delta-coupled-cluster calculations of K-edge core-ionization energies of third-row elements. *Phys. Chem. Chem. Phys.* **2022**, *24*, 13587−13596.
(35) Arias-Martinez, J. E.; Cunha, L. A.; Oosterbaan, K. J.; Lee, J.; Head-Gordon, M. Accurate core excitation and ionization energies from a state-specific coupled-cluster singles and doubles approach. *Phys. Chem. Chem. Phys.* **2022**, *24*, 20728−20741.
(36) Lee, J.; Small, D. W.; Head-Gordon, M. Excited states via coupled cluster theory without equation-of-motion methods: Seeking higher roots with application to doubly excited states and double core hole states. *J. Chem. Phys.* **2019**, *151*, 214103.
(37) Arias-Martinez, J. E.; Cunha, L. A.; Oosterbaan, K. J.; Lee, J.; Head-Gordon, M. Accurate core excitation and ionization energies from a state-specific coupled-cluster singles and doubles approach. *Phys. Chem. Chem. Phys.* **2022**, *24*, 20728−20741.
(38) Musiał, M.; Kucharski, S. A.; Bartlett, R. J. Equation-of-motion coupled cluster method with full inclusion of the connected triple excitations for ionized states: IP-EOM-CCSDT. *J. Chem. Phys.* **2003**, *118*, 1128−1136.
(39) Asthana, A.; Liu, J.; Cheng, L. Exact two-component equation-of-motion coupled-cluster singles and doubles method using atomic mean-field spin-orbit integrals. *J. Chem. Phys.* **2019**, *150*, 074102.
(40) Liu, J.; Matthews, D.; Coriani, S.; Cheng, L. Benchmark Calculations of K-Edge Ionization Energies for First-Row Elements Using Scalar-Relativistic Core-Valence-Separated Equation-of-Motion Coupled-Cluster Methods. *J. Chem. Theory Comput.* **2019**, *15*, 1642−1651.
(41) Aoki, T.; Ohno, K. Accurate quasiparticle calculation of x-ray photoelectron spectra of solids. *J. Phys.: Condens. Matter* **2018**, *30*, 21LT01.
(42) Golze, D.; Wilhelm, J.; van Setten, M. J.; Rinke, P. Core-Level Binding Energies from GW: An Efficient Full-Frequency Approach within a Localized Basis. *J. Chem. Theory Comput.* **2018**, *14*, 4856−4869.
(43) Golze, D.; Keller, L.; Rinke, P. Accurate Absolute and Relative Core-Level Binding Energies from GW. *J. Phys. Chem. Lett.* **2020**, *11*, 1840−1847.
(44) Mejia-Rodriguez, D.; Kunitsa, A.; Aprà, E.; Govind, N. Basis Set Selection for Molecular Core-Level GW Calculations. *J. Chem. Theory Comput.* **2022**, *18*, 4919−4926.
(45) Mejia-Rodriguez, D.; Kunitsa, A.; Aprà, E.; Govind, N. Scalable Molecular GW Calculations: Valence and Core Spectra. *J. Chem. Theory Comput.* **2021**, *17*, 7504−7517.
(46) Besley, N. A. Density Functional Theory Calculations of Core-Electron Binding Energies at the K-Edge of Heavier Elements. *J. Chem. Theory Comput.* **2021**, *17*, 3644−3651.
(47) Kahk, J. M.; Lischner, J. Accurate absolute core-electron binding energies of molecules, solids, and surfaces from first-principles calculations. *Phys. Rev. Mater.* **2019**, *3*, 100801.
(48) Ozaki, T.; Lee, C.-C. Absolute Binding Energies of Core Levels in Solids from First Principles. *Phys. Rev. Lett.* **2017**, *118*, 026401.
(49) Sun, J.; Ruzsinszky, A.; Perdew, J. P. Strongly Constrained and Appropriately Normed Semilocal Density Functional. *Phys. Rev. Lett.* **2015**, *115*, 036402.
(50) Xu, Q.; Prendergast, D.; Qian, J. Real-Space Pseudopotential Method for the Calculation of 1s Core-Level Binding Energies. *J. Chem. Theory Comput.* **2022**, *18*, 5471−5478.
(51) Gilbert, A. T. B.; Besley, N. A.; Gill, P. M. W. Self-consistent field calculations of excited states using the maximum overlap method (MOM). *J. Phys. Chem. A* **2008**, *112*, 13164−13171.
(52) Ye, H.-Z.; Welborn, M.; Ricke, N. D.; Van Voorhis, T. σ-SCF: A direct energy-targeting method to mean-field excited states. *J. Chem. Phys.* **2017**, *147*, 214104.

https://doi.org/10.1021/acs.jctc.4c00535
J. Chem. Theory Comput. 2024, 20, 6134−6143

(53) Ye, H.-Z.; Van Voorhis, T. Half-Projected σ Self-Consistent Field For Electronic Excited States. *J. Chem. Theory Comput.* **2019**, *15*, 2954−2965.
(54) Pehlke, E.; Scheffler, M. Evidence for site-sensitive screening of core holes at the Si and Ge (001) surface. *Phys. Rev. Lett.* **1993**, *71*, 2338−2341.
(55) Cho, J.-H.; Jeong, S.; Kang, M.-H. Final-state pseudopotential theory for the Ge 3d core-level shifts on the Ge/Si(100)-(2{}1) surface. *Phys. Rev. B Condens. Matter* **1994**, *50*, 17139−17142.
(56) Pasquarello, A.; Hybertsen, M. S.; Car, R. Theory of Si 2p core-level shifts at the Si(001)-SiO_2 interface. *Phys. Rev. B Condens. Matter* **1996**, *53*, 10942−10950.
(57) Rignanese, G.-M.; Pasquarello, A.; Charlier, J.-C.; Gonze, X.; Car, R. Nitrogen Incorporation at Si-SiO_2 Interfaces: Relation between N s Core-Level Shifts and Microscopic Structure. *Phys. Rev. Lett.* **1997**, *79*, 5174−5177.
(58) Haerle, R.; Riedo, E.; Pasquarello, A.; Baldereschi, A. sp^2/sp^3 hybridization ratio in amorphous carbon from C 1s core-level shifts: X-ray photoelectron spectroscopy and first-principles calculation. *Phys. Rev. B Condens. Matter* **2001**, *65*, 045101.
(59) Birgersson, M.; Almbladh, C.-O.; Borg, M.; Andersen, J. N. Density-functional theory applied to Rh(111) and CO/Rh(111) systems: Geometries, energies, and chemical shifts. *Phys. Rev. B Condens. Matter* **2003**, *67*, 045402.
(60) Schillinger, R.; Sljivancanin, Z.; Hammer, B.; Greber, T. Probing enantioselectivity with x-ray photoelectron spectroscopy and density functional theory. *Phys. Rev. Lett.* **2007**, *98*, 136102.
(61) Baraldi, A.; Bianchettin, L.; Vesselli, E.; de Gironcoli, S.; Lizzit, S.; Petaccia, L.; Zampieri, G.; Comelli, G.; Rosei, R. Highly under-coordinated atoms at Rh surfaces: interplay of strain and coordination effects on core level shift. *New J. Phys.* **2007**, *9*, 143.
(62) Han, J.; Chan, T.-L.; Chelikowsky, J. R. Quantum confinement, core level shifts, and dopant segregation in P-doped {Si}<110 > nanowires. *Phys. Rev. B Condens. Matter* **2010**, *82*, 153413.
(63) García-Gil, S.; García, A.; Ordejón, P. Calculation of core level shifts within DFT using pseudopotentials and localized basis sets. *Eur. Phys. J. B* **2012**, *85*, 239.
(64) Hait, D.; Head-Gordon, M. Orbital Optimized Density Functional Theory for Electronic Excited States. *J. Phys. Chem. Lett.* **2021**, *12*, 4517−4529.
(65) Hait, D.; Head-Gordon, M. Highly Accurate Prediction of Core Spectra of Molecules at Density Functional Theory Cost: Attaining Sub-electronvolt Error from a Restricted Open-Shell Kohn-Sham Approach. *J. Phys. Chem. Lett.* **2020**, *11*, 775−786.
(66) Cunha, L. A.; Hait, D.; Kang, R.; Mao, Y.; Head-Gordon, M. Relativistic Orbital-Optimized Density Functional Theory for Accurate Core-Level Spectroscopy. *J. Phys. Chem. Lett.* **2022**, *13*, 3438−3449.
(67) Hamann, D. R.; Schlüter, M.; Chiang, C. Norm-Conserving Pseudopotentials. *Phys. Rev. Lett.* **1979**, *43*, 1494−1497.
(68) Xu, Q.; Wang, S.; Xue, L.; Shao, X.; Gao, P.; Lv, J.; Wang, Y.; Ma, Y. Ab initio electronic structure calculations using a real-space Chebyshev-filtered subspace iteration method. *J. Phys.: Condens. Matter* **2019**, *31*, 455901.
(69) Epifanovsky, E.; Gilbert, A. T. B.; Feng, X.; Lee, J.; Mao, Y.; Mardirossian, N.; Pokhilko, P.; White, A. F.; Coons, M. P.; Dempwolff, A. L.; Gan, Z.; Hait, D.; Horn, P. R.; Jacobson, L. D.; Kaliman, I.; Kussmann, J.; Lange, A. W.; Lao, K. U.; Levine, D. S.; Liu, J.; McKenzie, S. C.; Morrison, A. F.; Nanda, K. D.; Plasser, F.; Rehn, D. R.; Vidal, M. L.; You, Z.-Q.; Zhu, Y.; Alam, B.; Albrecht, B. J.; Aldossary, A.; Alguire, E.; Andersen, J. H.; Athavale, V.; Barton, D.; Begam, K.; Behn, A.; Bellonzi, N.; Bernard, Y. A.; Berquist, E. J.; Burton, H. G. A.; Carreras, A.; Carter-Fenk, K.; Chakraborty, R.; Chien, A. D.; Closser, K. D.; Cofer-Shabica, V.; Dasgupta, S.; de Wergifosse, M.; Deng, J.; Diedenhofen, M.; Do, H.; Ehlert, S.; Fang, P.-T.; Fatehi, S.; Feng, Q.; Friedhoff, T.; Gayvert, J.; Ge, Q.; Gidofalvi, G.; Goldey, M.; Gomes, J.; González-Espinoza, C. E.; Gulania, S.; Gunina, A. O.; Hanson-Heine, M. W. D.; Harbach, P. H. P.; Hauser, A.; Herbst, M. F.; Hernández Vera, M.; Hodecker, M.; Holden, Z. C.; Houck, S.; Huang, X.; Hui, K.; Huynh, B. C.; Ivanov, M.; Jász, Á.; Ji, H.; Jiang, H.; Kaduk, B.; Kähler, S.; Khistyaev, K.; Kim, J.; Kis, G.; Klunzinger, P.; Koczor-Benda, Z.; Koh, J. H.; Kosenkov, D.; Koulias, L.; Kowalczyk, T.; Krauter, C. M.; Kue, K.; Kunitsa, A.; Kus, T.; Ladjánszki, I.; Landau, A.; Lawler, K. V.; Lefrancois, D.; Lehtola, S.; Li, R. R.; Li, Y.-P.; Liang, J.; Liebenthal, M.; Lin, H.-H.; Lin, Y.-S.; Liu, F.; Liu, K.-Y.; Loipersberger, M.; Luenser, A.; Manjanath, A.; Manohar, P.; Mansoor, E.; Manzer, S. F.; Mao, S.-P.; Marenich, A. V.; Markovich, T.; Mason, S.; Maurer, S. A.; McLaughlin, P. F.; Menger, M. F. S. J.; Mewes, J.-M.; Mewes, S. A.; Morgante, P.; Mullinax, J. W.; Oosterbaan, K. J.; Paran, G.; Paul, A. C.; Paul, S. K.; Pavošević, F.; Pei, Z.; Prager, S.; Proynov, E. I.; Rák, Á.; Ramos-Cordoba, E.; Rana, B.; Rask, A. E.; Rettig, A.; Richard, R. M.; Rob, F.; Rossomme, E.; Scheele, T.; Scheurer, M.; Schneider, M.; Sergueev, N.; Sharada, S. M.; Skomorowski, W.; Small, D. W.; Stein, C. J.; Su, Y.-C.; Sundstrom, E. J.; Tao, Z.; Thirman, J.; Tornai, G. J.; Tsuchimochi, T.; Tubman, N. M.; Veccham, S. P.; Vydrov, O.; Wenzel, J.; Witte, J.; Yamada, A.; Yao, K.; Yeganeh, S.; Yost, S. R.; Zech, A.; Zhang, I. Y.; Zhang, X.; Zhang, Y.; Zuev, D.; Aspuru-Guzik, A.; Bell, A. T.; Besley, N. A.; Bravaya, K. B.; Brooks, B. R.; Casanova, D.; Chai, J.-D.; Coriani, S.; Cramer, C. J.; Cserey, G.; DePrince, A. E., 3rd; DiStasio, R. A., Jr; Dreuw, A.; Dunietz, B. D.; Furlani, T. R.; Goddard, W. A., 3rd; Hammes-Schiffer, S.; Head-Gordon, T.; Hehre, W. J.; Hsu, C.-P.; Jagau, T.-C.; Jung, Y.; Klamt, A.; Kong, J.; Lambrecht, D. S.; Liang, W.; Mayhall, N. J.; McCurdy, C. W.; Neaton, J. B.; Ochsenfeld, C.; Parkhill, J. A.; Peverati, R.; Rassolov, V. A.; Shao, Y.; Slipchenko, L. V.; Stauch, T.; Steele, R. P.; Subotnik, J. E.; Thom, A. J. W.; Tkatchenko, A.; Truhlar, D. G.; Van Voorhis, T.; Wesolowski, T. A.; Whaley, K. B.; Woodcock, H. L., 3rd; Zimmerman, P. M.; Faraji, S.; Gill, P. M. W.; Head-Gordon, M.; Herbert, J. M.; Krylov, A. I.; et al. Software for the frontiers of quantum chemistry: An overview of developments in the Q-Chem 5 package. *J. Chem. Phys.* **2021**, *155*, 084801.
(70) Perdew, J. P.; Burke, K.; Ernzerhof, M. Generalized Gradient Approximation Made Simple. *Phys. Rev. Lett.* **1996**, *77*, 3865−3868.
(71) Dunning, T. H., Jr Gaussian basis functions for use in molecular calculations. I. contraction of (9s5p) atomic basis sets for the first-row atoms. *J. Chem. Phys.* **1970**, *53*, 2823−2833.
(72) Troullier, N.; Martins, J. L. Efficient pseudopotentials for plane-wave calculations. *Phys. Rev. B Condens. Matter* **1991**, *43*, 1993−2006.
(73) Fuchs, M.; Scheffler, M. Ab initio pseudopotentials for electronic structure calculations of poly-atomic systems using density-functional theory. *Comput. Phys. Commun.* **1999**, *119*, 67−98.
(74) Devlin, S. W.; Jamnuch, S.; Xu, Q.; Chen, A. A.; Qian, J.; Pascal, T. A.; Saykally, R. J. Agglomeration Drives the Reversed Fractionation of Aqueous Carbonate and Bicarbonate at the Air-Water Interface. *J. Am. Chem. Soc.* **2023**, *145*, 22384−22393.
(75) Becke, A. D. Density-functional thermochemistry. III. The role of exact exchange. *J. Chem. Phys.* **1993**, *98*, 5648−5652.
(76) Ambroise, M. A.; Jensen, F. Probing Basis Set Requirements for Calculating Core Ionization and Core Excitation Spectroscopy by the Δ Self-Consistent-Field Approach. *J. Chem. Theory Comput.* **2019**, *15*, 325−337.
(77) Hait, D.; Head-Gordon, M. Excited State Orbital Optimization via Minimizing the Square of the Gradient: General Approach and Application to Singly and Doubly Excited States via Density Functional Theory. *J. Chem. Theory Comput.* **2020**, *16*, 1699−1710.
(78) Foster, J. M.; Boys, S. F. Canonical Configurational Interaction Procedure. *Rev. Mod. Phys.* **1960**, *32*, 300−302.
(79) Makov, G.; Payne, M. C. Periodic boundary conditions in ab initio calculations. *Phys. Rev. B Condens. Matter* **1995**, *51*, 4014−4022.
(80) Payne, M. C.; Teter, M. P.; Allan, D. C.; Arias, T. A.; Joannopoulos, J. D. Iterative minimization techniques for ab initio total-energy calculations: molecular dynamics and conjugate gradients. *Rev. Mod. Phys.* **1992**, *64*, 1045−1097.
(81) Castro, A.; Rubio, A.; Stott, M. J. Solution of Poisson's equation for finite systems using plane-wave methods. *Can. J. Phys.* **2003**, *81*, 1151−1164.

https://doi.org/10.1021/acs.jctc.4c00535
J. Chem. Theory Comput. 2024, 20, 6134−6143

(82) Travnikova, O.; Børve, K. J.; Patanen, M.; Söderström, J.; Miron, C.; Sæthre, L. J.; Mårtensson, N.; Svensson, S. The ESCA molecule—Historical remarks and new results. *J. Electron Spectrosc. Relat. Phenom.* **2012**, *185*, 191−197.
(83) Siegbahn, K. M. G.; Price, W. C.; Turner, D. W. A Discussion on photoelectron spectroscopy - Electron spectroscopy for chemical analysis (e.s.c.a.). *Philos. Trans. R. Soc. London A* **1970**, *268*, 33−57.
(84) Biesinger, M. C.; Payne, B. P.; Grosvenor, A. P.; Lau, L. W. M.; Gerson, A. R.; Smart, R. S. C. Resolving surface chemical states in XPS analysis of first row transition metals, oxides and hydroxides: Cr, Mn, Fe, Co and Ni. *Appl. Surf. Sci.* **2011**, *257*, 2717−2730.
(85) Xie, S.; Liu, L.; Lu, Y.; Wang, C.; Cao, S.; Diao, W.; Deng, J.; Tan, W.; Ma, L.; Ehrlich, S. N.; Li, Y.; Zhang, Y.; Ye, K.; Xin, H.; Flytzani-Stephanopoulos, M.; Liu, F. Pt Atomic Single-Layer Catalyst Embedded in Defect-Enriched Ceria for Efficient CO Oxidation. *J. Am. Chem. Soc.* **2022**, *144*, 21255−21266.
(86) Corcoran, C. J.; Tavassol, H.; Rigsby, M. A.; Bagus, P. S.; Wieckowski, A. Application of XPS to study electrocatalysts for fuel cells. *J. Power Sources* **2010**, *195*, 7856−7879.
(87) Kahk, J. M.; Lischner, J. Combining the Δ-Self-Consistent-Field and GW Methods for Predicting Core Electron Binding Energies in Periodic Solids. *J. Chem. Theory Comput.* **2023**, *19*, 3276−3283.
(88) Hossain, M. S.; Dhillon, G. S.; Liu, L.; Sridhar, A.; Hiennadi, E. J.; Hong, J.; Bare, S. R.; Xin, H.; Ericson, T.; Cozzolino, A.; Khatib, S. J. Elucidating the role of Fe-Mo interactions in the metal oxide precursors for Fe promoted Mo/ZSM-5 catalysts in non-oxidative methane dehydroaromatization. *Chem. Eng. J.* **2023**, *475*, 146096.
(89) Van Speybroeck, V.; Hemelsoet, K.; Joos, L.; Waroquier, M.; Bell, R. G.; Catlow, C. R. A. Advances in theory and their application within the field of zeolite chemistry. *Chem. Soc. Rev.* **2015**, *44*, 7044−7111.
(90) Kim, S.; Lee, M.-S.; Camaioni, D. M.; Gutiérrez, O. Y.; Glezakou, V.-A.; Govind, N.; Huthwelker, T.; Zhao, R.; Rousseau, R.; Fulton, J. L.; Lercher, J. A. Self-Organization of 1-Propanol at H-ZSM-5 Brønsted Acid Sites. *JACS Au* **2023**, *3*, 2487−2497.
(91) Huang, Z.-Q.; Liu, L.-P.; Qi, S.; Zhang, S.; Qu, Y.; Chang, C.-R. Understanding All-Solid Frustrated-Lewis-Pair Sites on CeO2 from Theoretical Perspectives. *ACS Catal.* **2018**, *8*, 546−554.

https://doi.org/10.1021/acs.jctc.4c00535
J. Chem. Theory Comput. 2024, 20, 6134−6143